Accepted Manuscript

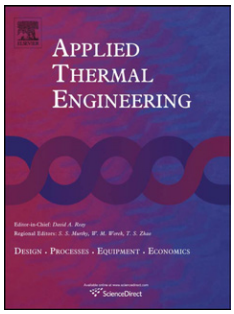

Title: Methodology for the estimation of cylinder inner surface temperature in an air-cooled engine

Authors: Elisa Carvajal Trujillo, Francisco J. Jiménez-Espadafor, José A. Becerra Villanueva, Miguel Torres García

PII: S1359-4311(11)00034-2

DOI: 10.1016/j.applthermaleng.2011.01.025

Reference: ATE 3389

To appear in: *Applied Thermal Engineering*

Received Date: 25 June 2010

Revised Date: 10 January 2011

Accepted Date: 15 January 2011

Please cite this article as: E.C. Trujillo, F.J. Jiménez-Espadafor, J. Becerra Villanueva, M.T. García. Methodology for the estimation of cylinder inner surface temperature in an air-cooled engine, Applied Thermal Engineering (2011), doi: 10.1016/j.applthermaleng.2011.01.025

Methodology for the estimation of cylinder inner surface temperature in an air-cooled engine

Elisa Carvajal Trujillo[*]*, Francisco J. Jiménez-Espadafor, José A. Becerra Villanueva, Miguel Torres García*

Thermal Power Group, Department of Energy Engineering, University of Seville

Escuela Técnica Superior de Ingenieros, Camino de los Descubrimientos, s/n. 41092 Sevilla, Spain.

*Corresponding author. Tel.:+34954486111; fax: +34954487243; elisa@esi.us.es.

Abstract

A methodology for the estimation of the mean temperature of the cylinder inner surface in an air-cooled internal combustion engine is proposed. Knowledge of this temperature is necessary to determine the heat flux from the combustion chamber to the cylinder wall. Along with the heat transfer coefficient this parameter also allows almost 50% of engine heat losses to be determined. The temperature is relatively easy to determine for water-cooled engines but this is not in the case for air-cooled engines. The methodology described here combines numerical and experimental procedures. Simulations were based on FEM models and experiments were based on the use of thermocouples and infrared thermography. The methodology avoids the use of data or correlations developed for other engines, providing more reliable results than extrapolating models from one engine to another. It also prevents from taking measurements from inside the combustion chamber, reducing invasion and experiments complexity. The proposed methodology has been successfully applied to an air-cooled four-stroke direct-injection diesel engine and it allows the cylinder mean inner surface temperature and cylinder-cooling air heat transfer coefficient to be estimated.

Keywords

air-cooled engine; heat transfer; cylinder temperature; infrared thermography.

Nomenclature

$C_{p,j}$	specific heat of cooling air at partition *i (j = i)* or at the outlet fan *(j=fan)* (J/kgK)
i	*partition (i* = 1, 2, 3, 4 correspond to the cylinder and *i* = 5, 6, 7 to the head)
$h_{ext,cyl}$	cylinder-cooling air heat transfer coefficient (W/m^{2}K)
m	*component: cylinder (m=cyl) or head (m=head)*
$\dot{m}_{exhaust,i}$	cooling air exhaust mass flow at partition *i* (kg/s)
$\dot{m}_{exhaust,m}$	cooling air exhaust mass flow of component *m* (kg/s)
$\dot{m}_{fuel}$	fuel flow (g/s)
n	number of points of comparison
p_{envir}	environmental pressure (bar)
$\dot{Q}_{cooling,m}$	time and spatially averaged heat flow from coolant side wall of the component *m* to the cooling air (J/s)
$\dot{Q}_{rejected,cyl}$	time and spatially averaged heat flow through the walls of the cylinder (J/s)
$\dot{q}_{rejected,cyl}$	heat flux from the combustion chamber and piston to the cylinder inner surface cylinder (W/m^2)
R_a	specific gas constant of air (m^2/Ks^2)
s	mean square error
S_i	section area of partition *i* (m^2)
$T_{exhaust,i}$	cooling air exhaust temperature at partition *i* (ºC)
$T_{exhaust,m}$	cooling air exhaust temperature of component *m* (ºC)
T_{fan}	cooling air temperature after fan (ºC)
$T_{surf,measured,k}$	measured coolant-side surface temperature at location *k* (ºC)
$T_{surf,sim,k}$	FEM simulated coolant-side surface temperature at location *k* (ºC)
$\bar{T}_{surf,inner,cyl}$	inner surface cylinder mean temperature (ºC)
$v_{exhaust,i}$	cooling air exhaust speed at partition *i* (m/s)

$[K]$	heat conduction matrix
$\{N\}$	vector of nonlinear heat flows
$\{P\}$	vector of applied heat flux
$[\Re]$	radiation exchange matrix
T_{abs}	absolution temperature
$\{u\}$	vector of grip point temperature

1. Introduction

Knowledge of heat transfer in internal combustion engines is important to understand such systems [1, 2] and it contributes to engine development, processes simulation and emissions reduction. In addition, it is important to guarantee the durability of engine components, avoid engine body distortions and improve engine design related to weight and auxiliary energy consumption.

Engine heat transfer phenomena have been studied extensively for many decades [3-8]. Numerous mathematical models have been proposed, including correlations based on dimensional analysis, which are widely accepted and, although they propose different heat fluxes, their evolution over the cycle is similar [7-8]. Many of these models include the gas-side wall temperature as a variable to obtain the heat flux through the chamber walls [7]. In addition, computational fluid dynamics (CFD) and/or finite element method (FEM) codes used for heat transfer simulations require the estimation of this temperature to provide boundary conditions. Convergence is attained through an iterative process. [9-10]. Furthermore, thermal analyses require the gas side wall temperature to evaluate temperature distribution and the thermomechanical behaviour of components [11-13]. Other heat transfer analyses use the lumped capacitance method and also need the mean gas side temperature [14-15]. Even with very precise functions, it is not possible to obtain accurate heat flux [7,16] unless accurate wall temperature measurements are available.

Some authors approximate the mean temperature of the distribution by one or more –few- local measures obtained by thermocouples [1,11,17]. These approaches implicitly assume errors that

can be acceptable for heat balances but can involve uncertainties in simulation cycles or temperature distribution analyses. It should be noticed that some authors, after having identified one correlation for one small-scale air-cooled engine [18], acknowledge that those correlation parameters are not valid for another small scale air-cooled engine with similar characteristics [19].

In most heat transfer analyses the external surface temperatures are not measured. For example, in the case of water-cooled engines, this temperature is often assumed to be equal to the coolant temperature or is calculated from hypotheses that are specific for water-cooled engines [15] and normally assume constant temperature for all operating points. This approach can not be extrapolated to air-cooled engines because the temperature field in the inner surface changes with the operating conditions [19]. Very few studies concerning heat transfer in air-cooled engines have been published and most of them consider two-stroke and/or spark-ignition engines [19-21].

In this paper a methodology for an air-cooled four-stroke direct injection diesel engine is proposed. This approach is based on simple energy balances and FEM simulations that use boundary conditions obtained experimentally from thermography, thermocouples and other sensors, while avoiding correlations or experimental data from other researchers. The proposed methodology has been successfully validated, as described in Section 6.

2. Engine description and experimental procedure

The experimental investigation was conducted on a four-stroke single-cylinder direct-injection (DI) compression ignition engine. The main characteristics of this engine are given in Table 1.

TABLE 1

The experimental measurements covered three engine speeds, namely 1800, 2400 and 2700 rpm, and in each case four different loads were considered – namely 25%, 50%, 75% and 100% of full engine load. Fuel flow, engine rpm and torque were simultaneously measured through all engine load conditions. Environmental pressure and relative humidity were measured using a barometer and a hygrometer, respectively.

The cooling air is driven by a fan mounted on the flywheel, Fig. 1. A cowling that surrounds the engine fins routes all of the cooling air to an outlet port. An adiabatic plate was installed in order to separate the head and cylinder air cooling flows. The outgoing flow and temperature were measured at 7 points in the discharge area, four of which correspond to the cylinder and the other three to the head, Fig. 2.

Air speed, $v_{exhaust,i}$, and temperature, $T_{exhaust,i}$, were measured at the centre of each partition "*i*" with an anemometer/temperature probe. The cooling air exhaust mass flow at partition "*i*", $\dot{m}_{exhaust,i}$, was evaluated by Eq. (1). The cooling air exhaust mass flow, $\dot{m}_{exhaust,m}$, and temperature, $T_{exhaust,m}$, were evaluated by Eqs. (2) and (3).

$$\dot{m}_{exhaust,i} = \frac{p_{envir} \cdot 10^5}{R_a \left(T_{exhaust,i} + 273\right)} v_{exhaust,i} S_i \qquad (1)$$

$$\dot{m}_{exhaust,cyl} = \sum_{i=1}^{i=4} \dot{m}_{exhaust,i} \qquad \dot{m}_{exhaust,head} = \sum_{i=5}^{i=7} \dot{m}_{exhaust,i} \qquad (2)$$

$$T_{exhaust,cyl} = \frac{\sum_{i=1}^{i=4} \dot{m}_{exhaust,i} \cdot T_{exhaust,i}}{\dot{m}_{exhaust,cyl}} \qquad T_{exhaust,head} = \frac{\sum_{i=5}^{i=7} \dot{m}_{exhaust,i} \cdot T_{exhaust,i}}{\dot{m}_{exhaust,head}} \qquad (3)$$

The cooling air temperature after the fan, T_{fan}, was averaged from readings from three thermocouples located in the same plane, Fig. 2.

Air temperatures, mass flow and heat flow from the coolant side wall of the cylinder to the cooling air for all engine conditions tested were obtained. The main results for the measured air cooling temperature (ºC), air mass flow (g/s) and heat flow from cylinder wall (J/s) are given in Table 2.

FIGURE 1

FIGURE 2

TABLE 2

Time and spatially averaged heat flow from the coolant side cylinder wall to the cooling air, $\dot{Q}_{cooling,cyl}$, was estimated experimentally from the difference in output and input enthalpy of the cooling air for each operating point, according to the First Law of Thermodynamics, Eq. (4). In this process kinetic energy changes were not considered. The inlet and outlet enthalpy values were obtained from the inlet and outlet temperatures, respectively, where $C_{p,i}$ is the specific heat of air in the grid *i* of the cylinder, under the conditions considered, and $C_{p,fan}$ is the specific heat of air at the outlet fan, under the conditions considered. The heat losses were evaluated and represented less than 1% of the total.

$$\dot{Q}_{cooling,cyl} = \sum_{i=1}^{i=4} C_{p,i} T_{exhaust,i} \dot{m}_{exhaust,i} - C_{p,fan} T_{fan} \dot{m}_{exhaust,cyl} \quad (4)$$

Coolant side surface temperature, $T_{surf,measured,k}$, values were obtained by thermography and thermocouples for all conditions tested. The selection of a greater number of points would be expected to provide better results. If all temperatures are measured with thermocouples the installation would be extremely complex and there would be a risk of failure or the mass flow path could even be affected. As a result, the temperatures were also measured with a thermal camera and this leads to minimal invasion. This approach allows more temperatures to be registered without affecting the cooling air flow. Holes of 20 mm diameter were drilled in the cowling. In order to minimise invasion these holes remained capped when thermograms were not being recorded. Six infrared inspection holes were drilled to register the temperatures of 14 surface locations. Five thermocouples were placed at the bottom fins at the points where the thermograms were unreliable because of the poor angle of vision or the presence of accessories that interfered image acquisition. Therefore, temperatures at 19 locations were measured. The distribution of the holes and the measurement points is represented in Fig. 3.

FIGURE 3

Temperature measurement by infrared cameras is a very complex process that is influenced by the environment and the atmosphere. Furthermore, this technique requires parameters that are difficult to measure. In this regard, a set of standards was followed. In order to avoid surface

temperature measurement errors due to emissivity the contact and non-contact methods were followed [22]. The emissivity was experimentally measured to be equal to 0.85 using a tape with known emissivity, a contact thermocouple and a sample of the metal of the cylinder that was heated in a furnace. The reflector method [23] was used to avoid measurement errors from the reflected infrared energy from heating sources. This method was applied in each engine operating point. During the experiments the most important heat sources that might disturb the experiment, e.g. exhaust duct, were shielded. Standards in [24-25] were used to ensure that the experimental procedure and devices (ThermaCAM PM695) were suitable to obtain the measures.

3. Proposed methodology

The methodology proposed to determine the cylinder inner surface mean temperature is based on an inverse method that solves the heat flux components by a steady state heat transfer FEM. The steady state heat balance equation is given by Eq. (5). The equilibrium equation is solved by a Newton iteration.

$$[K]\{u\}+[\Re]\{u+T_{abs}\}^4=\{P\}+\{N\} \quad (5)$$

One of the main difficulties associated with FEM concerns the correct imposition of boundary conditions [7]. As boundary conditions were imposed the estimated value of heat flow through the internal walls of the cylinder $\dot{Q}_{rejected,cyl}$, T_{fan}, $T_{exhaust,cyl}$ and the convection coefficient on finned surfaces of the cylinder, $h_{ext,cyl}$. The proposed methodology employed an iterative process to determine $h_{ext,cyl}$ and this converged when temperatures of the coolant side surfaces given by the FEM simulation, $T_{surf,sim,k}$, matched the measured values, $T_{surf,measured,k}$, Fig. 4.

Thus, $h_{ext,cyl}$ and the inner surface cylinder mean temperature, $\overline{T}_{surf,inner,cyl}$, were obtained for each operating point.

FIGURE 4

The characteristic dimensions of this cylinder are: 95 mm diameter, 180 mm length, 150 mm width and 172 mm height. There are 14 fins of 4 mm width with gaps of 7 mm between each. Several mesh sizes were tested being finally adopted the best compromise between resolution and computational time execution. For example, Fig. 5 show two simple models of one fin with different size mesh. Both FEM simulation results were compared with the known analytical solutions. It was noted that the both absolute and relative errors in both cases very low. Although the errors decreased with the mesh size, this difference is not worth the effort in the meshing and simulation time, Table 3. The maximum size of the element edge is imposed to be 7 mm and there are at least 3 elements of each length. The total number of 3D elements is 54285 (TETRA4) and 19827 nodes and the resolution time is ≈ 500 seconds in a Windows XP based PC, Fig. 6. The material is cast iron with a conductivity of 51.9 W/mK and this remains constant in the temperature range 50-200 ºC.

FIGURE 5

TABLE 3

FIGURE 6

5. Application of boundary conditions

FEM boundary conditions have to be suitable to ensure goods results. There is a limited set of possible boundaries that can be established using different conditions such as temperatures on surfaces, heat fluxes and convection coefficient. The first attempt involved setting temperatures on the outer surfaces and a suitable heat flux distribution on the inner surfaces. However, the first of the above boundary conditions was impossible to implement due to the lack of information on the temperature field across the entire surface – the temperature of only 10% of the surface was measured. Even in the best case, thermography can only register visible surfaces and the lateral surfaces of the fins were not exposed. An interpolation for each fin, from the extreme temperatures, would be a long and complex process.

The second attempt to set boundary conditions was as follows, Fig. 7:

- heat flux from the combustion chamber and piston to the cylinder inner surface, $\dot{q}_{rejected,cyl}$, which is explained in section 5.1;
- $h_{ext,cyl}$, and;
- the air temperature was assumed to evolve in a linear manner from the measured inlet (T_{fan}) to outlet ($T_{exhaust,cyl}$) temperatures.

Moreover, $T_{surf,measured,k}$ were used for validation of the coefficient $h_{ext,cyl}$.

FIGURE 7

5.1. Heat flux to cylinder inner surface, $\dot{q}_{rejected,cyl}$:

A steady state balance was carried out for the energy fluxes in the cylinder, where $\dot{Q}_{cooling,cyl}$ is equal to $Q_{rejected,cyl}$, which is the total heat flux to inner cylinder surface. This is integrated by heat flux from combustion chamber gases plus heat flux from piston surfaces in contact with cylinder inner surface. The heat exchanged longitudinally between the cylinder and the head was assumed to be negligible. This parameter is more relevant as the area of finned surface increases and the thickness of the cylinder decreases.

The imposition of boundary conditions in the FEM model requires the heat flux per unit time and area. This flow is called $\dot{q}_{rejected,cyl}$ and is related to $\dot{Q}_{rejected,cyl}$ by Eq. (6):

$$\dot{Q}_{rejected,cyl} = \int_{Area} \dot{q}_{rejected,cyl} dA \qquad (6)$$

Although the heat flux is known, it is not possible to estimate experimentally the flux distribution. In an effort to analyze the relevance of this flux distribution on cylinder temperature, three different flux distributions were simulated. These distributions are axisymmetric in all cases and exterior unfinned surfaces and their corresponding inner surface were assumed to be adiabatic, Fig. 7. This assumption is reasonable because inner adiabatic surfaces are never exposed to combustion chamber gases.

The configurations considered were as follows: (a) uniform; (b) linear distribution, with slope equal to the temperature variation on the outer surfaces; and (c) linear distribution, with slope opposite to the previous case.

The temperature simulation results for the three heat flux distributions, corresponding to 1800 rpm and 25% load, are shown in Fig. 8. It can be appreciated that temperature distribution hardly varies from case to case. More specifically, the maximum temperature variation, evaluated as temperature difference at the same surface point, is 3.0% between cases (a) and (b) and 4.6% between cases (a) and (c). With respect to the average temperature of the inner surface on which the heat flux is applied, the variation between the three cases is even lower; for example, between cases (a) and (b) the variation is only 1.0% and between (a) and (c) it is 1.4%. The temperature simulation results for the three heat flux distributions analyzed are shown in Fig. 8. Since the three cases provide similar temperature distributions, option a) was preferred for simplicity in the imposition of the boundary conditions.

FIGURE 8

6. Methodology validation and results

Once the boundary conditions (uniform heat flux on the elements of the inner surface of the cylinder and convection coefficient on the finned surface elements) had been imposed, the model was analyzed using the NX/NASTRAN® solver module.

When the simulation had finished it was sent to the FEMAP® post-processing module in order to obtain the temperatures of the finned external surfaces and, in turn, validate the convection coefficient. A set of 19 points was chosen to compare the temperatures $T_{surf,measured,k}$ with $T_{surf,sim,k}$, Fig. 3. The positions of these points on the outer finned surface are shown in the figure and these points are distributed throughout the four sides of the cylinder.

A mean square error was calculated and this was denoted by the letter *s* and defined by Eq. (7), where *n* is the number of points of comparison. The method identified the value of $h_{ext,cyl}$ that minimizes the mean square error from temperature measurements [26, 27].

$$s = \sqrt{\frac{\sum_{k=1}^{k=n}\left(T_{surf,sim,k} - T_{surf,measured,k}\right)^2}{n-1}} \quad (7)$$

The determination of the optimal value of $h_{ext,cyl}$ follows the iterative scheme described in Fig. 9. The iterations start by estimating ten (10) values of $h_{ext,cyl}$ from previous knowledge. For each of them, the FEM is simulated and the corresponding s are evaluated. Pairs ($h_{ext,cyl}$, s) comprise the data set, DS. A rough version of curve $s = f\left(h_{ext,cyl}\right)$ is obtained by cubic interpolation using the current data set. This allows identifying the minimum of f, $s_{\min} = f\left(DS\right)$. Then, a new FEM is simulated with the $h_{ext,cyl}$ coming from the previous step and its corresponding s is evaluated. If $\left|\left(s - s_{\min}\right)/s\right|$ >5% convergence is not attained and the new pair $\left(h_{ext,cyl}, s\right)$ is incorporated into DS to refine the estimation of the curve in next iteration. If it is lower than 5%, the convergence is warranted and the last value of $h_{ext,cyl}$ is taken as the actual cylinder-cooling air heat transfer coefficient.

FIGURE 9

A plot of measured versus simulated temperatures at 19 points for all the engine operating points tested is shown in Fig. 10. It can be observed that the error is small and represents a uniform percentage throughout all the tests being a bit higher in areas near the exhaust side, which have higher temperatures

FIGURE 10

The heat transfer coefficients and values for parameter *s* are given in Table 4 for all tests. As expected, for all load conditions the heat transfer coefficient increased with engine speed, with a maximum observed at 75% load. These values are consistent with previously published results [28].

After validation, $\bar{T}_{surf,inner,cyl}$ was obtained and these data are presented in Fig. 11.

FIGURE 11

Mean temperature and engine speed vary in a nonlinear fashion; the higher the engine speed the lower the mean temperature of the cylinder gas-side surface. Different factors can be considered to determine this behaviour and the most relevant are:

- Cooling air is blown by a fan where mass flow and outlet pressure are an almost linear function and a quadratic function of engine speed, respectively. Therefore, as the engine speed increases, the cylinder-cooling air heat transfer coefficient increases, thus reducing external thermal resistance.
- Turbulence inside the combustion chamber increases in a nonlinear fashion with engine speed, thus increasing the combustion gases/inner wall heat transfer coefficient and therefore reducing internal thermal resistance. In addition, the combustion chamber is of the bowl in piston type, which promotes high swirling flow close to top dead centre and therefore increases the heat transfer coefficient.
- The engine used in the study did not have advanced injection control. Therefore, as the engine speed increases the delay in the start of combustion also increases, and this in turn changes the temperature evolution of the gases throughout the engine cycle.

7. Conclusions

A methodology is proposed that is based on temperature measurements carried out by thermography and thermocouples. The method was validated in a mono-cylinder diesel research engine by calculation of cylinder mean inner surface temperature and cylinder-air cooling heat transfer coefficient. It was found that almost 50% of the total engine heat losses come from the cylinder.

As expected for this air-cooled engine, the mean temperature of the cylinder gas side wall depends on engine load and speed. The mean temperature and engine load vary almost

linearly and have a positive relationship. This behaviour can be explained as being due to the larger amount fuel injected into the combustion chamber as the engine load increases. As a result, more energy flows as heat losses to the cylinder wall and, finally, to the cooling air. Higher relative heat losses (heat losses divided by injected fuel) occur as the injected fuel decreases.

Mean temperature and engine speed vary in a nonlinear fashion; the higher the engine speed the lower the mean temperature of the cylinder gas-side surface. That is related with the increase of the cooling air flow and the turbulence when engine speed increases.

The cylinder-cooling air heat transfer coefficient for every engine load condition tested was estimated and good agreement was obtained with the expected results. These results are also consistent with literature work. This coefficient increases continuously with engine speed at every engine load in an almost linear fashion, as expected, and it has a maximum with engine load for every engine speed.

Work is in progress aimed at using the same methodology for the evaluation of heat losses throughout the engine head.

Acknowledgements

The work in this paper is a part of project CTQ2007-68026-CO2-02/PPQ within the I+D+i National Plan in the period 2007–2009 and was backed by the Spanish Government (Ministry of Science and Education). The authors are grateful to the Ministry of Science and Education of Spain for their financial support.

References

[1] J.B. Heywood, Internal Combustion Engines Fundamentals, McGraw Hill Book Company, New York, 1989.

[2] R. Stone, Introduction to Internal Combustion Engines, Macmillan Press Ltd., 1999.

[3] C.F. Taylor and T.Y. Toong Heat transfer in internal-combustion engines, ASME paper 57-HT-17, 1957.

[4] G.A. Woschni, Universally applicable equation for the instantaneous heat transfer coefficient in the internal combustion engine,. SAE 670931, 1967.

[5] G.F. Hohenberg, Advance approaches for heat transfer calculation, SAE 790825, 1979.

[6] J. Chang, O. Güralp, Z. Filipi, D. Assanis, T. Kuo, P. Najt and R. Rask, New heat transfer correlation for an HCCI engine derived from measurements of instantaneous surface heat flux, SAE 2004-01-2996.

[7] G. Borman and K. Nishiwaki, Internal combustion engine heat transfer, Progress in Energy and Combustion Science, Vol. 13, nº 1, 1987, 1-46.

[8] P. Tamilporai, N, Baluswamy, P. Mannar Jawahar, S. Subramaniyam, S. Chandrasekaran, K. Vijayan, S. Jaichandar, J. Janci Rani, K. Arunachalam, Simulation and analysis of combustion and heat transfer in low heat rejection diesel engine using two zone combustion model and different heat transfer models, SAE 2003-01-1067.

[9] V. Esfahanian, A. Javheri, M. Ghaffarpour, Thermal analysis of an SI engine piston using different combustion boundary condition treatments, Applied Thermal Engineering, 26, 2006, 277-287.

[10] A. Jafari, S. K. Hannani, Effect of fuel and engine operational characteristics on the heat loss from combustion chamber surfaces of SI engines, International Communications in Heat and Mass Transfer, Vol 33, Issue 1, 2006, 122-134.

[11] C.H. Li, Piston thermal deformation and friction considerations, SAE 20086, 1982.

[12] R. Keribar and T. Morel, Methods for thermomechanical analysis of thermal barrier coatings in diesel engines, Surface and Coatings Technology, Vol. 30, Issue 1, 1987, 63-71.

[13] E. Buyukkaya and M. Cerit, Thermal analysis of a ceramic coating diesel engine piston using 3-D finite element method, Surface and Coatings Technology, Vol. 202, Issue 2, 2007, 398-402.

[14] D.M. Baker and D.N. Assanis, A methodology for coupled thermodynamic and heat transfer analysis of a diesel engine, Applied Mathematical Modelling, Vol. 18, Issue 11, 1994, 590-601.

[15] S.V. Bohac, D.M. Baker and D.N. Assanis, A Global Model for Steady State and Transient S.I. Engine Heat Transfer Studies, SAE 960073.

[16] A.J. Torregrosa, P. Olmeda, B. Degraeuwe and M.A. Reyes, A concise wall temperature model for DI Diesel engines, Applied Thermal Engineering 26 Issues 11-12, 2006, 1320-1327.

[17] 17B.R. Tillock and J.K. Martin, Measurement and modelling of thermal flows in an air cooled engine, SAE 961731, 1996.

[18] Y. Wu, B. Chen, Heat transfer model for small-scale spark-ignition four-stroke engines, International Journal of Heat and Mass Transfer, Vol 49, Issues 21-22, 2006, 3895-3905.

[19] Y. Wu, B. Chen, F. Hsieh and C. Ke, Heat transfer model for small-scale spark-ignition engines, International Journal of Heat and Mass Transfer, Vol 52, Issues 7-8, 2009, 1875-1886.

[20] D. Descieux, M. Feidt, One zone thermodynamic model simulation of an ignition compression engine, Applied Thermal Engineering, Vol 27, Issues 8-9, 2007, 1457-1466.

[21] Y. Zhaoda, F. Zheng, Y. Siaoli, Y. Zhixing and S. Hongouan, Calculation and prediction of thermal loading of the air cooled diesel engine, SAE 881254, 1988.

[22] ASTM E1933 - 99a(2005)e1 Standard Test Methods for Measuring and Compensating for Emissivity Using Infrared Imaging Radiometers.

[23] ASTM E1862 - 97(2002)e1 Standard Test Methods for Measuring and Compensating for Reflected Temperature Using Infrared Imaging Radiometers.

[24] ASTM E1213 - 97(2009) Standard Test Method for Minimum Resolvable Temperature Difference for Thermal Imaging Systems.

[25] ASTM E1311 - 89(2004) Standard Test Method for Minimum Detectable Temperature Difference for Thermal Imaging Systems.

[26] D.C. Montgomery and E.A. Peck, Introduction to Linear Regression Analysis, New York Willey 2º Edition, 1992.

[27] Appendix B. Review of probability and statistics, International Geophysics, Vol. 90, 2005, 251-272.

[28] D.J. Thornhill, Experimental investigation into the temperature and heat transfer distribution around air – cooled cylinders, SAE 2006-32-0039, 2006.

> We propose a methodology for heat transfer calculation. > The analysis is based in cylinder of internal combustion engines. > We combine FEM and thermography technique for surface temperature measurement.> We avoid intrusive technique measurements.

Type	**DI mono cylinder** **4 stroke**
Combustion chamber	Bowl in piston
Cylinder displacement	708 cm^3
Bore	95 mm
Stroke	100 mm
Compression ratio	19.2:1
Maximum power	11 kW at 3000 rpm
Maximum torque	45 Nm at 2100 rpm
Fuel	Diesel EN 590
Charging	Naturally aspirated
Lubrication	Gear oil pump
Injection pump	Mechanical
Refrigeration	Air

Table 1. Deutz FL1 906 engine characteristics.

load	25%	50%	75%	100%
1800 rpm	[54, 101, 2820]	[57, 100, 3017]	[61, 100, 3251]	[64, 100, 3856]
2400 rpm	[51, 146, 3170]	[60, 151,3562]	[57, 148, 4510]	[67, 147, 5132]
2700 rpm	[47, 175, 3550]	[47, 180, 4105]	[57, 184, 5489]	[60, 184, 6378]

Table 2. Results for the operating conditions,

$[T_{exhaust,cyl}$ (ºC), $\dot{m}_{exhaust,cyl}$ (g/s), $\dot{Q}_{cooling,cyl}$ (J/s)]

	Node	"x" (mm)	Analytical T (ºC)	Simulation FEM T (ºC)	ε_{abs} (ºC)	ε_{rel} (%)
20 mm mesh size element	1	0	100.0	100.0	0	0
	2	20	75.2	75.4	0.2	0.3
	3	40	60.0	60.4	0.3	0.5
	4	60	51.9	52.2	0.3	0.6
	5	80	49.2	49.6	0.3	0.7
10 mm mesh size element	1	0	100.0	100.0	0	0
	2	10	86.2	86.2	0.03	0.04
	3	20	75.2	75.3	0.05	0.07
	4	30	66.6	66.7	0.06	0.10
	5	40	60.1	60.1	0.07	0.12
	6	50	55.2	55.3	0.08	0.14
	7	60	51.9	52.0	0.08	0.16
	8	70	49.9	50.0	0.08	0.17
	9	80	49.2	49.3	0.08	0.17

Table 3. Comparison between known and simulation results for 10 and 20 mm mesh sizes.

load	25%	50%	75%	100%
1800 rpm	[146, 8.7]	[170, 9.6]	[150, 12.2]	[123, 14.5]
2400 rpm	[200, 9.1]	[213, 9.5]	[233, 12.0]	[186, 17.4]
2700 rpm	[239, 11.8]	[230, 11.7]	[250, 11.6]	[200, 18.1]

Table 4: Results of the iteration process, [$h_{ext,cyl}$ (W/m^{2}K), s].

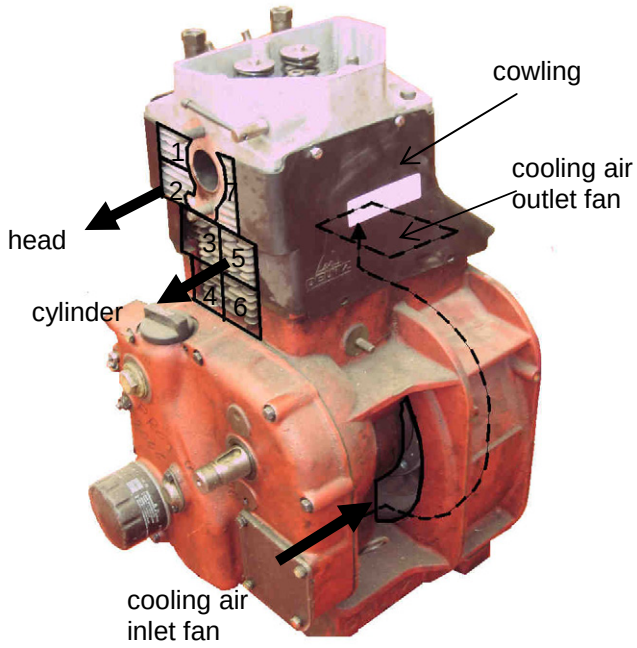

Fig. 1. Visualization of air cooling flow and grids

(cylinder: 1–4 and head: 5–7).

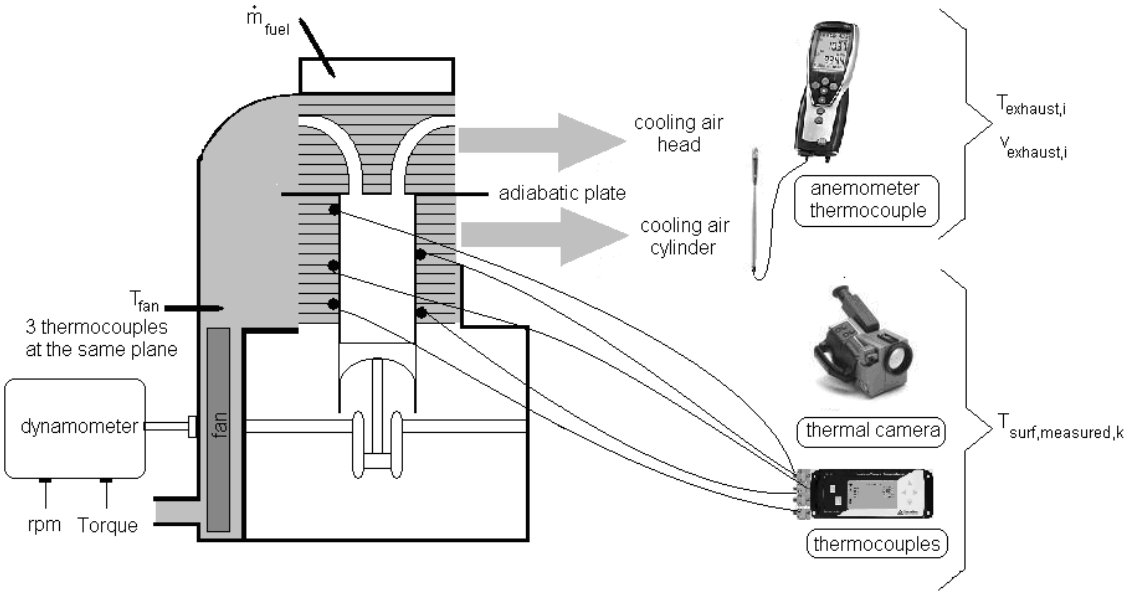

Fig. 2. Experimental set-up.

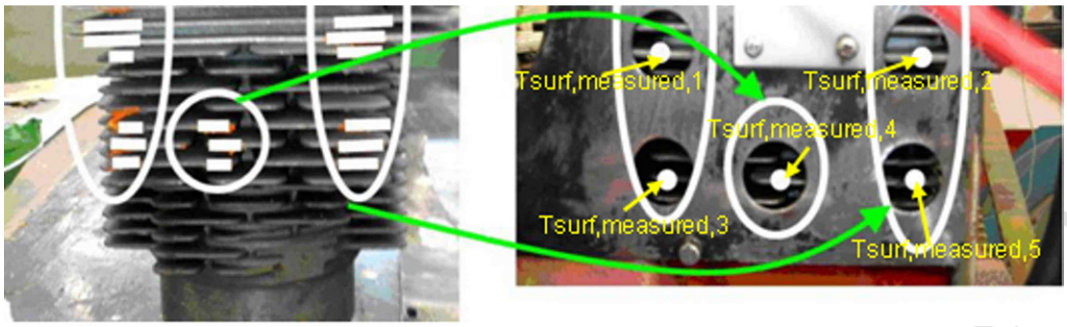

Fig. 3. Cylinder injector side showing the cylinder surfaces that are visible through the holes (white bands) and points chosen for thermographic evaluation (circles).

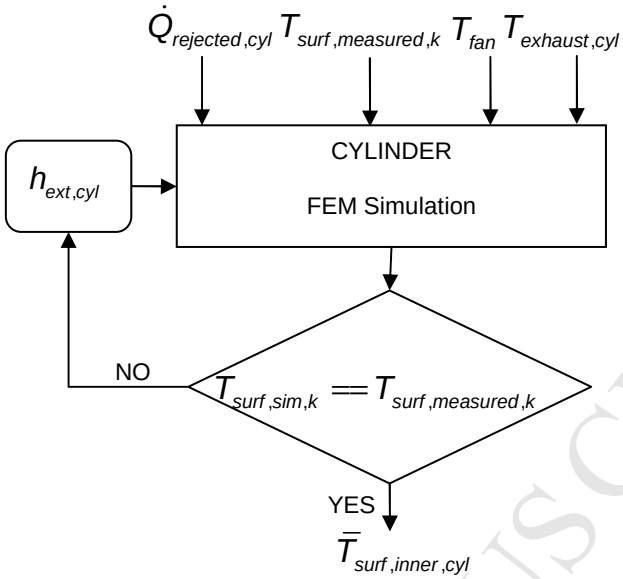

Fig. 4. Iterative process for the determination of cylinder mean inner surface temperature and cylinder-air cooling heat transfer coefficient.

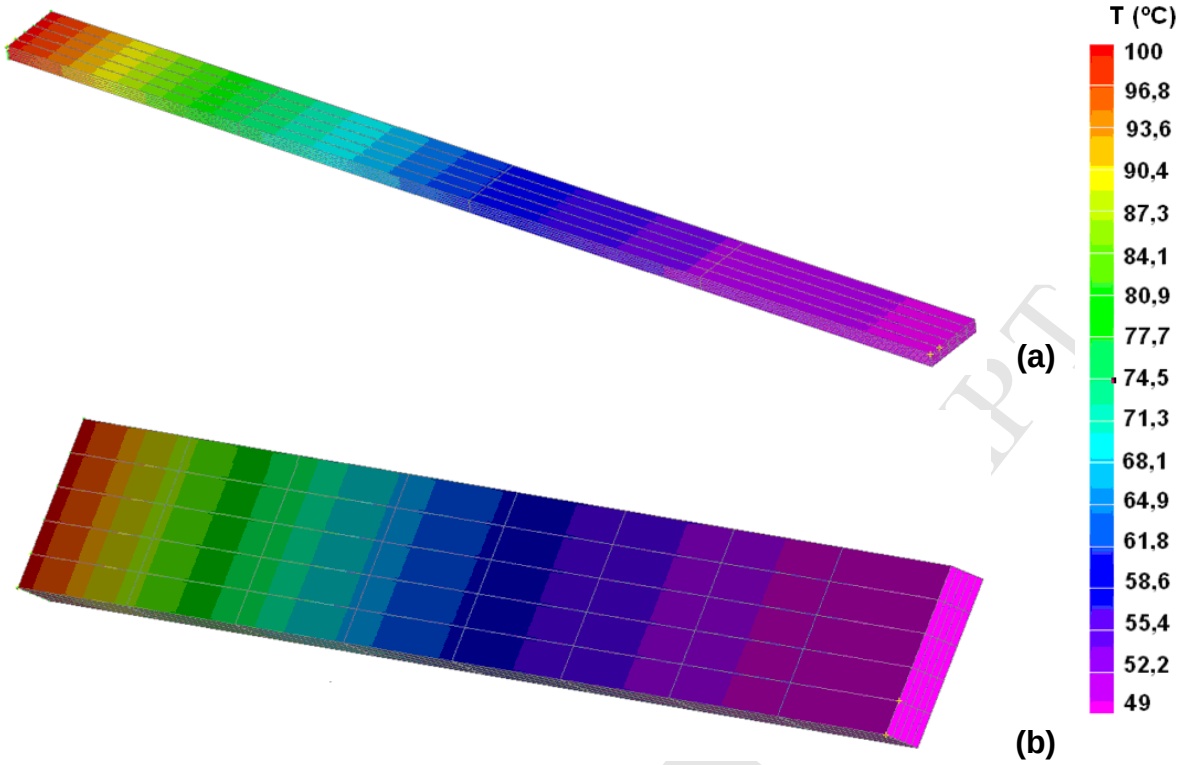

Fig. 5. Simulated temperature distribution for 20 mm (a) and 10 mm (b) size element.

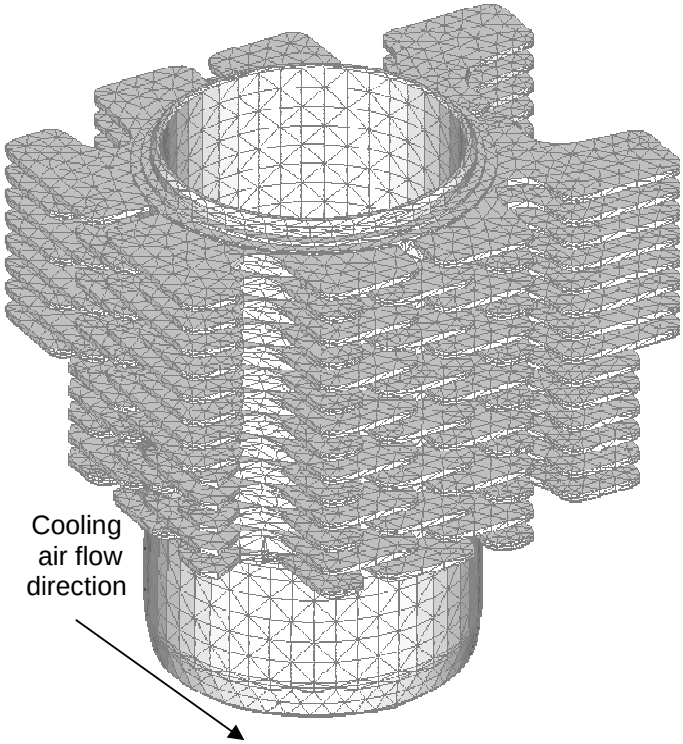

Fig. 6. Mesh of cylinder model.

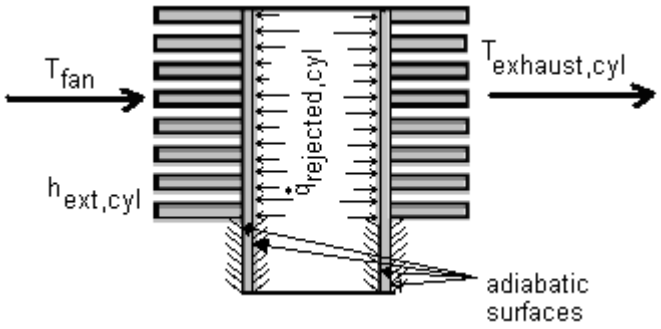

Fig. 7. Boundary conditions of the cylinder model.

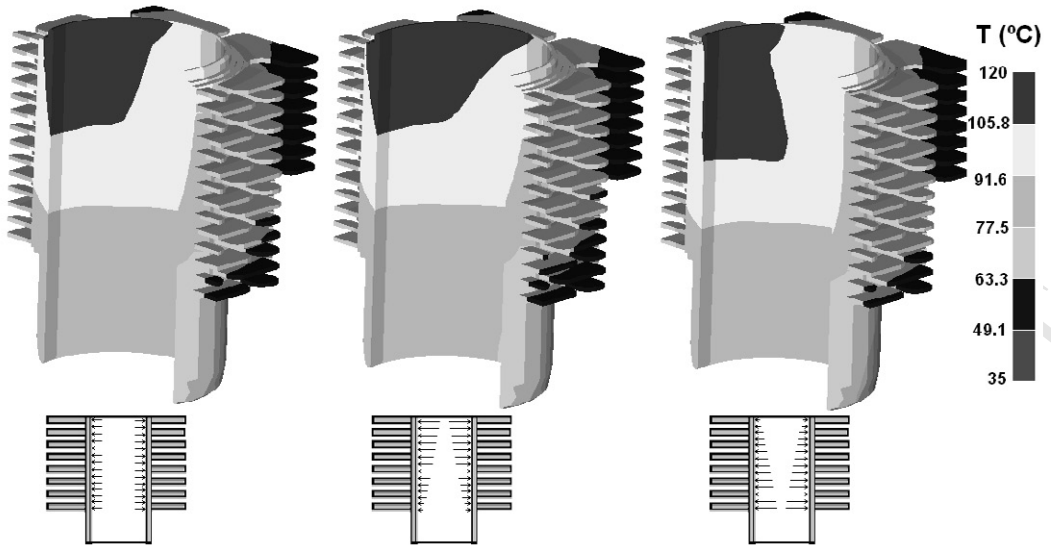

(a) uniform (b) positive slope 31º (c) negative slope –31º

Fig. 8. Temperature distribution (top) for the three heat fluxes considered (bottom).

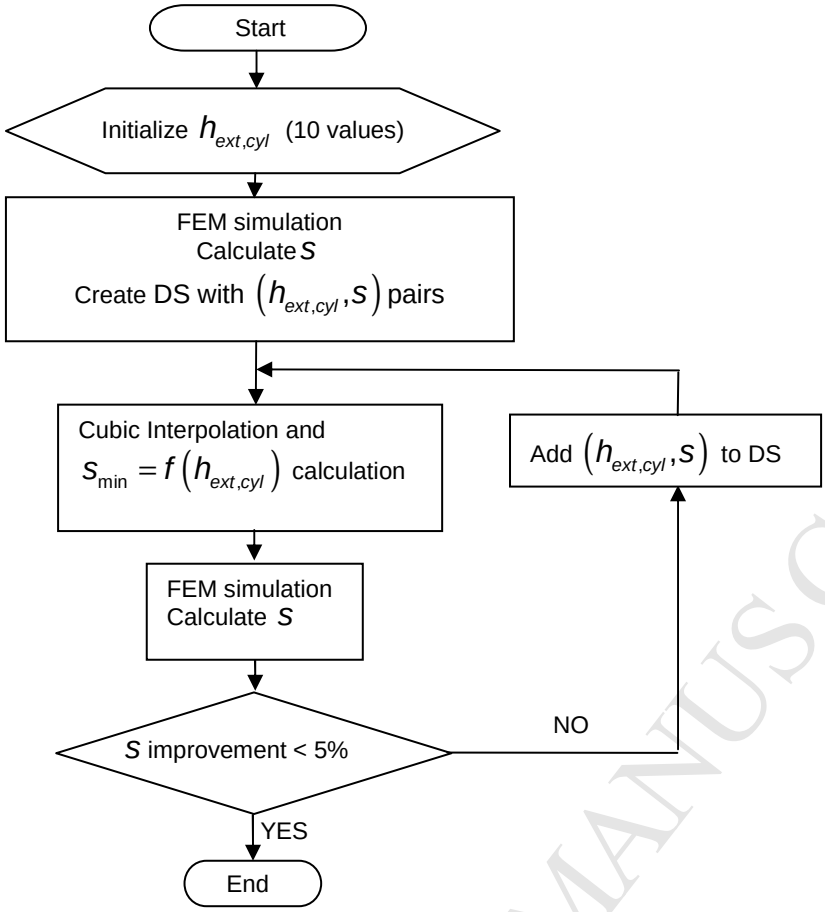

Fig. 9: $h_{ext,cyl}$ iteration process.

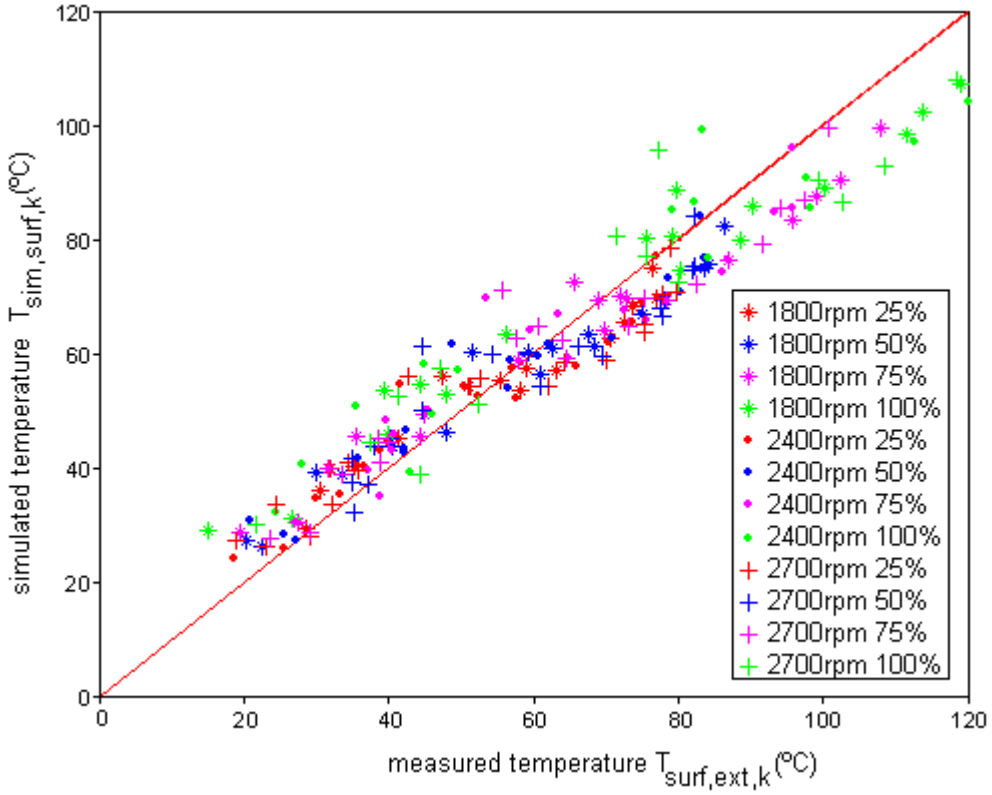

Fig. 10. Representation of the temperatures at the points of comparison.

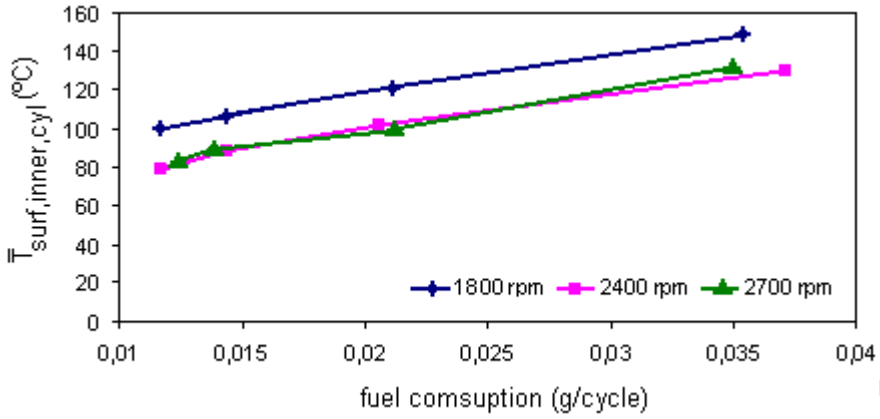

Fig. 11. Estimated inner surface cylinder mean temperature.